



Universität Stuttgart

iew
Institut für
Elektrische Energiewandlung

Berichte aus dem Institut für Elektrische Energiewandlung

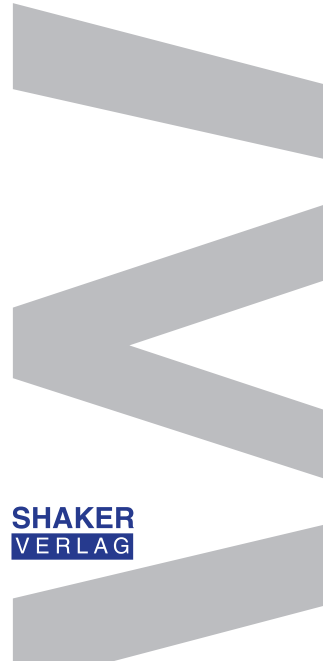
Jonathan Terfurth

Integrated Multi-Motor Actuators for Medical
and Industrial Robotics



Band 13

**SHAKER
VERLAG**



**Integrated Multi-Motor Actuators for
Medical and Industrial Robotics**

**Von der Fakultät Informatik, Elektrotechnik
und Informationstechnik der Universität Stuttgart
zur Erlangung der Würde des Doktor-Ingenieurs (Dr.-Ing.)
genehmigte Abhandlung**

**Vorgelegt von
Jonathan Theo Terfurth
aus Bonn**

**Hauptberichterin: Prof. Dr.–Ing. Nejila Parspour
Mitberichter: Prof. Dr. Andrew McDaid**

Tag der mündlichen Prüfung: 09.03.2022

**Institut für Elektrische Energiewandlung
der Universität Stuttgart**

2022

Berichte aus dem Institut für Elektrische Energiewandlung

Band 13

Jonathan Terfurth

**Integrated Multi-Motor Actuators for Medical
and Industrial Robotics**

D 93 (Diss. Universität Stuttgart)

Shaker Verlag
Düren 2023

Bibliographic information published by the Deutsche Nationalbibliothek

The Deutsche Nationalbibliothek lists this publication in the Deutsche Nationalbibliografie; detailed bibliographic data are available in the Internet at <http://dnb.d-nb.de>.

Zugl.: Stuttgart, Univ., Diss., 2022

Copyright Shaker Verlag 2023

All rights reserved. No part of this publication may be reproduced, stored in a retrieval system, or transmitted, in any form or by any means, electronic, mechanical, photocopying, recording or otherwise, without the prior permission of the publishers.

Printed in Germany.

ISBN 978-3-8440-9050-5

ISSN 2196-9213

Shaker Verlag GmbH • Am Langen Graben 15a • 52353 Düren

Phone: 0049/2421/99011-0 • Telefax: 0049/2421/99011-9

Internet: www.shaker.de • e-mail: info@shaker.de

Preface

This thesis emerged during my work as a research associate at the Institute of Electrical Energy Conversion at the University of Stuttgart and as part of the International Research Training Group *Soft Tissue Robotics* (GRK 2198/1, funded by the German Research Foundation (Deutsche Forschungsgemeinschaft)) of which I was an associated doctoral research member.

I want to express a special thanks to Prof. Dr.-Ing. Nejila Parspour, who encouraged and supported me throughout my thesis as my main doctoral supervisor and examiner and overall during my time and work at the institute.

Also, I wish to thank Prof. Dr. Andrew McDaid for making my research stay with his group at the University of Auckland worthwhile on a thematic and personal level, as well as for being the co-examiner of this thesis.

For supporting me in every challenge large and small, personal or content-related alike, and also for becoming close friends, I want to thank my colleagues.

A big thank you also goes to the workshop staff, Herrmann Kattner in particular, without whom many aspects of this work would have been impossible.

The thesis students as well as research assistants who I supervised were also very helpful for the outcome of this thesis and I want to thank every one of them for their work.

The final big thank you goes to my family and friends who always supported me, did not hold back on telling me their opinions no matter what, and pushed me in achieving this thesis and doctoral degree.

Abstract

In this doctoral thesis, an integrated robotic joint actuator concept consisting of more than one distributed electromagnetic torque source is presented. It is stated where current robotic joint actuators are limited for certain applications and how the suggested concept can improve the behavior in those regards.

The joint actuator concept is formulated from the ground up, giving design guidelines and evaluating optimal topologies for certain applications. To reach the set goals of this thesis, the integration of mechanics, mostly in the form of a gearbox, and electromagnetic torque sources is advanced further than the typical state-of-the-art of robotic joint actuation. This is combined with the design of a small high-torque outer rotor motor and a control structure, thus enabling a multitude of operating strategies, specifically targeting aspects like high efficiency or output precision. Deep integration is, among other things, enabled by the evaluation of suitable materials.

Two different exemplary prototype designs with either distributed motors or distributed motorphases are suggested, including electromagnetic as well as mechanical design, and evaluated in detail. With the given multi-motor joint actuator design characteristics, these can be adapted to specific applications, for example by changing the underlying topology or the electric drive topology.

Finalizing this thesis, an extensive evaluation of the made decisions and created designs is performed, based on which the overall concept is classified.

Zusammenfassung

In dieser Dissertation wird ein integriertes Robotergelenk-Aktuatorkonzept vorgestellt, das aus mehr als einer verteilten elektromagnetischen Drehmomentquelle besteht. Es wird aufgezeigt, bei welchen Anwendungen aktuelle Ansätze in welcher Hinsicht limitiert sind und wie das vorgeschlagene Konzept das Verhalten in diesen Bereichen verbessern kann.

Das Konzept des Gelenkaktuators wird von Grund auf definiert, wobei Designrichtlinien und optimale Topologien für spezifische Anwendungsfälle evaluiert werden. Auf dem Weg die Ziele dieser Arbeit zu erreichen wird die Integration von Mechanik, meist in Form eines Getriebes, und elektromagnetischer Drehmomentquellen weiter vorangetrieben, als es typischerweise dem aktuellen Stand der Technik in der Robotik entspricht. Dies wird kombiniert mit dem Design eines kleinen Außenläufermotors mit hohem Drehmoment sowie einer Regelungsstruktur, wodurch eine Vielzahl von Betriebsstrategien ermöglicht wird, die speziell auf Aspekte wie hohe Effizienz oder Präzision am Abtrieb ausgerichtet sind. Eine starke Integration wird unter anderem durch die Evaluierung geeigneter Materialien ermöglicht.

Es werden beispielhaft zwei unterschiedliche Prototypen zum einen mit verteilten Motoren und zum anderen mit verteilten Motorphasen auf elektromagnetischer und mechanischer Ebene ausgelegt und im Detail ausgewertet. Mit den gegebenen Charakteristiken der Mehrmotoren-Gelenkaktuatoren können diese an spezifische Anwendungen angepasst werden, zum Beispiel durch Variation der zugrunde liegenden Topologie oder Änderung der elektrischen Antriebstopologie.

Abgeschlossen wird diese Dissertation mit einer umfangreichen Auswertung und Bewertung der getroffenen Entscheidungen und entwickelten Konzepte, mit der das Gesamtkonzept eingeordnet wird.

Table of Contents

List of Abbreviations	XIII
List of Symbols	XV
List of Figures	XXI
List of Tables	XXV
List of Algorithms	XXVII
1 Introduction	1
1.1 Goal of this Doctoral Thesis	2
1.2 Project Environment <i>IRTG Soft Tissue Robotics</i>	3
2 Joint Actuation in Medical and Industrial Robotics	5
2.1 Robotic Joint Actuator Requirements	6
2.1.1 Torque	6
2.1.2 Rotational Speed & Dynamics	7
2.1.3 Weight & Size	7
2.1.4 Sensor Data & Interfaces	8
2.1.5 Efficiency	9
2.1.6 Control and Model Characteristics	9
2.2 Current Approaches and State of the Art of Robotic Joint Actuators	9
2.2.1 Typical Components and their Characteristics	10
2.2.2 Alternative Actuator Approaches	11
2.2.3 Specific Application Joint Actuator Concepts	12

3	Integrated Multi-Motor Robotic Joint Actuators	13
3.1	Concept overview	14
3.2	Input and Output Characteristic Options	16
3.2.1	Torque Distribution	17
3.2.2	Sun Gear Actuation	20
3.2.3	Planet Actuation	21
3.3	Advantages and Challenges of Multi-Motor Setups	22
3.3.1	Output Torque	23
3.3.2	Precision, Repeatability & Stiffness	24
3.3.3	Safety and Redundancy	25
3.3.4	Complexity	25
4	Material Evaluations	27
4.1	Stator & Rotor Materials	27
4.1.1	Experimental Magnetic Material Parameter Determination	30
4.1.2	Jiles-Atherton Parameter Determination	34
	Software Structure	35
	Parameter Determination Approach Interpretation	42
	Material Evaluation	42
4.2	Coil Materials and Manufacturing	47
5	Multi-Motor Prototypes	49
5.1	Definition of Requirements	50
5.2	Prototype <i>Distributed Motors</i>	51
5.2.1	Gear Design	51
5.2.2	Planet Motor Design	52
5.2.3	Mechanical Actuator Design	62
5.2.4	Electronics	65
5.2.5	Actuator Model	66
5.3	Prototype <i>Distributed Phases</i>	68
5.3.1	Gear Design	68
5.3.2	Transverse Flux Machine Electromagnetic Design	70
5.3.3	Materials	70
5.3.4	Mechanical Design	71
	Phase Rotor Bearing Mounting	73
	Phase Alignment	74
	Torsional Rigidity & Position Measurement	74

5.3.5	Simulative Preliminary Evaluation	75
5.3.6	Prototype Build	76
6	Control Options & Strategies	79
6.1	Joint Actuator Control	81
6.2	Torque Distribution	81
6.2.1	Static	82
6.2.2	Eliminate Torque Ripple	82
6.2.3	Precision, Repeatability & Eigenfrequency Shift . . .	83
6.2.4	Loss Minimization	84
6.2.5	Redundancy and Lifetime Improvements	85
6.2.6	Operating Condition Adaption	85
6.3	Low Level Current Control	85
7	Evaluation & Results	87
7.1	Test & Evaluation Environment	87
7.2	Single Planet Drive Motor	88
7.2.1	Mechanical Evaluation	88
	Moment of Inertia of Planet Drive Rotor	88
7.2.2	Electrical and Magnetic Circuit Evaluation	89
	Stator Phase Resistance	89
	Back Electromotive Force	90
	Magnet Operating Point and Demagnetization	92
7.2.3	Output Characteristics	92
	Torque	93
	Dynamic Behavior	94
	Short Circuit Behavior	94
	Efficiency and Losses	95
7.2.4	Conclusion for the Evaluation of a Single Planet Motor	97
7.3	Active Planetary Gear <i>Distributed Motors</i>	97
7.3.1	Mechanical	98
	Moment of Inertia	98
7.3.2	Magnetic	100
7.3.3	Output Characteristics	101
7.3.4	Gear Tensioning Control Strategy	103
7.3.5	Evaluation Summary Joint Actuator <i>Distributed Motors</i>	104

Table of Contents

7.4	Active Planetary Gear <i>Distributed Phases</i>	105
7.4.1	Electrical and Magnetic Circuit Evaluation	105
	Stator Phase Resistance and Inductance	105
	Back Electromotive Force	106
	Phase Offset	106
7.4.2	Output Characteristics	108
7.4.3	Magnetic	110
7.4.4	Efficiency	111
7.4.5	Evaluation Summary Joint Actuator <i>Distributed Phases</i>	112
8	Conclusion & Outlook	113
	Bibliography	115
A	Flow Charts & Algorithms	129
B	Jiles Atherton Parameter Estimation Application	133
C	Components <i>Distributed Motors</i>	135
D	Components <i>Distributed Phases</i>	151
E	Additional Evaluation Data Integrated Planet Drives	157

List of Abbreviations

Notation	Description
$_3D$	Three-Dimensional
AC	Alternating Current
BEMF	Back Electromotive Force
BLDC	Brushless DC
CAD	Computer-Aided Design
DC	Direct Current
DEA	Dielectric Elastomeric Actuator
DFG	German Research Foundation (Deutsche Forschungsgemeinschaft)
EDM	Electrical Discharge Machining
EM	Electrical Motor
FEA	Finite Element Analysis
FEM	Finite Element Method
GA	Genetic Algorithm
GUI	Graphical User Interface
HEV	Hybrid Electric Vehicle
HR	Hard Robot
IRTG	International Research Training Group

List of Abbreviations

Notation	Description
JA	Joint Actuator
JAM	Jiles-Atherton Model
LCM	Least Common Multiple
LUT	Lookup-table
MD	Main Drive
MOSFET	Metal–Oxide–Semiconductor Field-Effect Transistor
PC	Personal Computer
PCB	Printed Circuit Board
PD	Planet-Integrated Drive
PG	Planet Spur Gear
PGT	Planetary Gear Train
Ph.D.	Philosophical Doctorate
PID	Proportional–Integral–Derivative
PMSM	Permanent Magnet Synchronous Motor
RG	Ring Spur Gear
SFLA	Shuffled Frog Leaping Algorithm
SG	Sun Spur Gear
SLM	Selective Laser Melting
SMA	Shape-Memory Alloy
SMC	Soft Magnetic Composite
SR	Soft Robot
ST	Soft Tissue
STR	Soft Tissue Robotics
TFM	Transverse Flux Machine

List of Symbols

Symbol	Unit	Description
A	mm^2	Area
A_{cs}	mm^2	Cross section area
a_{JA}	$\text{\AA}/\text{m}$	Domain wall density, Jiles-Atherton model
B	T	Magnetic flux density
C_0	kN	Static bearing load rating
c_{JA}	—	Magnetization reversibility, Jiles-Atherton model
C_r	kN	Dynamic bearing load rating
d	mm	Distance
d_{act}	mm	Actuator diameter
d_{g}	mm	Air gap diameter
d_{i}	mm	Inner diameter
d_{o}	mm	Outer diameter
d_{PD}	mm	Active outer diameter planet drive
d_{pi}	mm	Gear pitch diameter
f	Hz	Frequency
f_{cog}	Hz	Mechanical cogging torque frequency
f_{cost}	—	Cost / objective function
F_r	kN	Radial bearing load
F_{rad}	N	Radial force component
g	—	Gear module
H	$\text{\AA}/\text{m}$	Magnetic field strength

List of Symbols

Symbol	Unit	Description
b	mm	Height
H_C	A/m	Magnetic coercitivity
b_{mag}	mm	Radial magnet height
H_{max}	A/m	Maximum magnetic field strength
I	A	Electrical current
I_1	A	Primary side current
i_{ph}	A	Electrical phase current
I	kg mm ²	Moment of inertia
I_{Cl}	kg mm ²	Moment of inertia of clutch
I_{IS}	kg mm ²	Moment of inertia of input shaft
I_{JA}	kg mm ²	Moment of inertia of joint actuator
I_{L1}	kg mm ²	Moment of inertia at gearbox level 1
I_{L2}	kg mm ²	Moment of inertia at gearbox level 2
I_{L3}	kg mm ²	Moment of inertia at gearbox level 3
I_{MA}	kg mm ²	Moment of inertia of main motor adapter
I_{MD}	kg mm ²	Moment of inertia of main motor rotor
I_{OS}	kg mm ²	Moment of inertia of output shaft
I_{PD}	kg mm ²	Moment of inertia of planet drive rotor
I_{PG}	kg mm ²	Moment of inertia of planet spur gear
I_{RG}	kg mm ²	Moment of inertia of ring spur gear
I_{SG}	kg mm ²	Moment of inertia of sun spur gear
J	T	Magnetic polarization
j_t	mm	Gear mesh allowance
k_{JA}	A/m	Pinning loss, Jiles-Atherton model
k_w	—	Winding factor
l	mm	Length
$l_{10\text{h}}$	s	Bearing lifetime
l_{act}	mm	Active length
l_{mag}	mm	Magnet radial length

Symbol	Unit	Description
l_{mp}	mm	Magnet path length
l_{PD}	mm	Active axial length planet drive
$l_{TFM,ph}$	mm	Active axial length transverse flux machine phase
L_{ph}	H	Phase inductance
M	A/m	Magnetization
m	—	Number of phases
M_{an}	A/m	Anhysteretic magnetization
M_{max}	A/m	Maximum magnetization
$M_{S,JA}$	A/m	Saturation magnetization, Jiles-Atherton model
n	1/min	Rotational speed
N_1	—	Number of toroidal core field winding turns
N_2	—	Number of toroidal core measure winding turns
n_{act}	1/min	Rotational actuator speed
N_c	—	Number of coil winding turns
$N_{c,1}$	—	Number of primary side coil winding turns
$N_{c,2}$	—	Number of secondary side coil winding turns
$N_{c,ph}$	—	Number of coil winding turns per phase
$N_{c,t}$	—	Number of coil winding turns per stator tooth
N_{gt}	—	Number of spur gear teeth
$N_{gt,PG}$	—	Number of planet spur gear teeth
$N_{gt,RG}$	—	Number of ring spur gear teeth
$N_{gt,SG}$	—	Number of sun spur gear teeth
N_S	—	Number of stator slots
p	—	Number of pole pairs
P_L	W	Power loss
$P_{L,Cu}$	W	Power loss in electrical conductors, copper losses
$P_{L,Iron}$	W	Power loss in soft magnetic components, iron losses
q	—	Slots per pole per phase
R	—	Mechanical reduction ratio

List of Symbols

Symbol	Unit	Description
R	Ω	Electrical resistance
r_{δ}	mm	Air gap radius
η_{ev}	s	Mechanical lever length
R_{MD}	—	Reduction ratio main drive to output
$R_{\text{MD,PD}}$	—	Reduction ratio main drive to planet drive
R_{PD}	—	Reduction ratio planet drive to output
R_{ph}	Ω	Electrical phase resistance
S	—	Safety coefficient
S_{F}	—	Safety coefficient gear breakage
S_{Fst}	—	Safety coefficient static deflection
S_{H}	—	Safety coefficient pitting
S_{Hst}	—	Safety coefficient static contact
T	Nm	Torque
t	s	Time
T_{cog}	Nm	Cogging torque
T_{JA}	Nm	Torque joint actuator
T_{MD}	Nm	Torque main drive
$T_{\text{MD,ref}}$	Nm	Reference torque main drive
T_{PD}	Nm	Torque planet drives
T_{PD1}	Nm	Torque planet drive 1
$T_{\text{PD1,ref}}$	Nm	Reference torque planet drive 1
T_{PD2}	Nm	Torque planet drive 2
$T_{\text{PD2,ref}}$	Nm	Reference torque planet drive 2
T_{PD3}	Nm	Torque planet drive 3
$T_{\text{PD3,ref}}$	Nm	Reference torque planet drive 3
T_{PD4}	Nm	Torque planet drive 4
$T_{\text{PD4,ref}}$	Nm	Reference torque planet drive 4
T_{ph}	Nm	Torque of a single phase
$T_{\text{RG,ref}}$	Nm	Reference torque at ring spur gear

Symbol	Unit	Description
$T_{\text{tilt,ph}}$	Nm	Tilting torque on integrated phases
V_2	V	Secondary side voltage
V_{DC}	V	DC-link voltage
V_i	V	Induced voltage
α_{JA}	—	Inter-domain coupling, Jiles-Atherton model
α_{PD}	rad/s^2	Mechanical angular acceleration planet drive
δ	mm	Air gap length
ΔT	%	Relative torque ripple
ε_{el}	rad	Electrical rotor angle
$\varepsilon_{\text{mech}}$	rad	Mechanical rotor angle
Θ	A	Magnetomotive force
κ	S/m	Electrical conductivity
μ	Vs/A m	Magnetic permeability
η	%	Efficiency
η_{g}	%	Gear efficiency
τ_{p}	mm	Pole pitch
Ω	rad/s	Mechanical angular velocity
χ_{an}	—	Magnetic susceptibility of anhysteretic curve
χ_{in}	—	Magnetic susceptibility of initial curve

List of Figures

3.1	Schematic mechanical concept drawing of the four-motor robotic actuator.	15
3.2	Schematics of gear topology variants.	16
3.3	Torque over motor diameter, normalized to axial length. . . .	18
3.4	Torque output per gear stage and overall over different reduction ratios.	20
3.5	Schematic mechanical concept drawing of the three-phase distributed robotic actuator.	22
4.1	Chemical composition for the evaluated materials.	30
4.2	Toroidal cores of Armco Pure Iron, 1.4104 steel and 1.0045. .	31
4.3	Reference magnetic field H with $f = 0.1$ Hz.	32
4.4	BH -curves including initial magnetization and hysteresis for respective materials.	33
4.5	Structure of Jiles-Atherton model parameter estimation implementation.	35
4.6	Visualization of toroidal core model design.	36
4.7	Visualization of Shuffled Frog Leaping Algorithm.	37
4.8	Visualization and calculation of least squared distance, Fréchet distance, and Gauss area similarity functions.	39
4.9	Approximation of $M_{S,JA}$ for 1.0045 and 1.7131 materials. . .	41
4.10	Convergence during parameter determination of the evaluated materials.	43
4.11	BH -comparison of measurement and simulation data after Jiles-Atherton model parameter fitting.	44
4.12	Relative and absolute error of simulated B characteristic curves over H compared to the experimental data.	46

4.13	3D-printed copper coils for five teeth and 15 teeth.	48
5.1	Harmonic frequencies of the two suitable slot pole topologies relative to mechanical rotational speed.	56
5.2	Reference and final geometry of integrated planet drive.	57
5.3	Phase interconnection printed circuit board 3D view.	59
5.4	Flux density B and magnetic flux lines and directions within finalized planet drive geometry, surrounded by the planet spur gear.	61
5.5	Magnetic pull on rotor ($\varepsilon_{\text{mech}} = 0$ rad) over air gap length and cumulated total torque and direction.	62
5.6	Mechanical concept of the five-motor robotic actuator.	63
5.7	Power electronics printed circuit board 3D view top and bottom.	66
5.8	Joint actuator model and structure overview.	67
5.9	Torque distribution for a 120 mm outer pitch diameter and active length of 10 mm integrated transverse flux machine.	69
5.10	Transverse flux machine geometry.	71
5.11	Mechanical concept of the five phase transverse flux machine.	72
5.12	Cross-section of integrated transverse flux machine phase.	73
5.13	Torque related electrical phase angle error $\Delta\varepsilon_{\text{el}}$, based on [JT5].	75
5.14	Flux density B in cross-sectional area of the designed transverse flux machine for one given position.	76
5.15	Components of planar TFM prototype and testing setup [JT5].	77
6.1	Distributed motor controller structure.	80
6.2	Static torque distribution between main drive and planet drives.	82
6.3	Torque distribution for increased gear stiffness, precision and repeatability.	83
6.4	Loss minimization torque distribution for main drive and respective planet drive torque.	84
7.1	Back electromotive force of motor <i>Variants 1, 4 and 5</i> at $n = 60$ 1/min and $n = 120$ 1/min.	91
7.2	Magnetic polarization and flux density for N42SH magnet at 80 °C and 120 °C and flux density in one magnet for a single exemplary time step during operation.	92
7.3	Cogging torque of planet drive <i>Variant 1</i>	93
7.4	Torque over time for $I = 3$ A and $n = 60$ 1/min for the different configurations V1 and V4.	94

7.5	Phase currents and output torque for short circuit at respective constant rotational speeds of $n = 15 \text{ }^1/\text{min}$, $n = 60 \text{ }^1/\text{min}$ and $n = 120 \text{ }^1/\text{min}$	95
7.6	Efficiency η of planet drive <i>Variant 1</i> for an extended operating range.	96
7.7	Losses P_L of planet drive <i>Variant 1</i> for an extended operating range.	96
7.8	Inertia over required joint actuator output torque.	100
7.9	Magnetic flux density B and magnetic flux lines for one given position of the full joint actuator.	101
7.10	Torque over electrical angle for separate motors and sum of all four planet drives.	102
7.11	Simulative evaluation of pre-tensioning control strategy.	104
7.12	Induced phase voltages for different rotational speeds [JT5].	107
7.13	Median, quartile, and whisker of electrical phase angle offset	107
7.14	Simulated torque of single TFM phase at rated phase current $i_{ph} = 10 \text{ A}$. The five-phase motor torque T is calculated in post-processing by summing up all five identical phases, offset by $\varepsilon_{el} = 72^\circ$, respectively [JT5].	108
7.15	Average actuator output torque T over current amplitude i_{ph} for different motor speeds n . All simulation curves consider a gear efficiency of $\eta_g = 95 \%$ [JT5].	109
7.16	Magnetic flux density of active components. Air, one stator-half (top) and one rotor (bottom right) are hidden [JT5].	110
7.17	Simulative efficiency of motor before gear stage and without friction losses for phase currents of 2 A to 20 A.	111
7.18	Simulated and measured actuator efficiency.	112
A.1	Flow chart of shuffled frog leaping algorithm.	130
B.1	Screenshot of designed application for determination of Jiles-Atherton model parameters.	134
C.1	Technical drawing: Planet spur gear.	136
C.2	Technical drawing: Ring spur gear.	137
C.3	Technical drawing: Planet carrier 1.	138
C.4	Technical drawing: Planet carrier 2.	139
C.5	Technical drawing: Torque input shaft.	140

C.6	Technical drawing: Torque output shaft adapter.	141
C.7	Technical drawing: Labyrinth seal.	142
C.8	Technical drawing: Main motor shaft adapter.	143
C.9	Technical drawing: Main motor shaft adapter.	144
C.10	Technical drawing: Stator lamination of planet motor.	145
C.11	Technical drawing: Rotor ring of planet motor.	146
C.12	Technical drawing: Stator flange.	147
C.13	Technical drawing: Sun gear position sensor.	148
C.14	Technical drawing: Sun gear position sensor magnet ring.	148
C.15	Technical drawing: Ring gear position sensor.	149
C.16	Technical drawing: Intermediate plate.	150
D.1	Technical drawing: Stator core half.	152
D.2	Technical drawing: Planet spur gear / rotor.	153
D.3	Technical drawing: Planet carrier.	154
D.4	Technical drawing: Output shaft.	155
E.1	BEMF of motor variant 2 at $n = 60 \frac{1}{\text{min}}$ and $n = 120 \frac{1}{\text{min}}$	158
E.2	BEMF of motor variant 3 at $n = 60 \frac{1}{\text{min}}$ and $n = 120 \frac{1}{\text{min}}$	158

List of Tables

3.1	Comparison of transverse flux motor topologies.	24
4.1	Toroidal core dimensions of prototype material selection.	31
4.2	Toroidal core material electrical conductivities.	34
4.3	Jiles-Atherton parameter determination search range.	40
4.4	Jiles-Atherton parameter determination boundary conditions.	42
4.5	Jiles-Atherton parameter identification of the pre-selected materials for evaluation and design.	45
5.1	Planetary gear train design characteristics.	52
5.2	Planet drive material configurations.	53
5.3	Planet drive target specifications.	54
5.4	Winding factor and cogging torque frequency for different slot pole combinations.	55
5.5	Different coil design characteristics.	59
5.6	Planet drive torque simulation results.	60
5.7	Maximum input power per spur gear within the epicyclic gearing and resulting safety coefficients.	65
5.8	Planetary gear train design characteristics distributed phases	69
7.1	Moment of inertia around rotational axis for different rotor materials and components.	89
7.2	Planet drive phase DC resistance at 20 °C.	90
7.3	Planet drive characteristic evaluated data.	97
7.4	Moment of inertia around respective component rotational axis for all rotating parts.	98
7.5	Planet drive phase resistance and inductance at 20 °C.	106

List of Algorithms

A.1	Quadrilateral Gauss area cost computation.	131
-----	--	-----